A Computational Study of a Supersonic Flow with Base Bleed

Young-Ki Lee†, Heuy-Dong Kim* and Srinivasan Raghunathan**

Base Bleed 를 가지는 초음속 유동에 대한 수치해석적 연구

이영기† · 김희동* · Srinivasan Raghunathan **

Key Words : Base Drag(베이스 항력), Base Bleed(베이스 블리드), Drag Reduction(항력 저감), Separation(박리), Supersonic Flow(초음속 유동)

Abstract

A numerical analysis has been performed to give an understanding of the physics of a compressible base flow with mass bleed in a Mach 2.47 freestream. Axisymmetric, compressible mass-averaged Navier-Stokes equations are computed using a two-equation turbulence model, standard k-ω, and a fully implicit finite volume scheme. The mass bleed is characterized by the change in the mass flow rate of the bleed jet non-dimensionalized by the product of the base area and freestream mass flux. The result showing that there is an optimum bleed condition with maximum base pressure, leading to a minimum base drag, is clearly predicted and the validation with experimental data shows reasonable agreement.

1. Introduction

Drag reduction has been one of the major issues in the design of aerodynamic bodies such as missiles, projectiles and rockets because these generally undergo significant deterioration of flight performance by drag. For the kinds of flight bodies mentioned above, especially, the drag in the base region has the significant contribution of to pressure drag. At transonic speeds, for example, base drag constitutes a major portion up to 50 % of the total drag for typical projectiles at Mach 0.9.[(1)] Therefore base drag should be considered separately from other components and considerable effort has been made to find suitable techniques for obtaining low base-drag shell design.

Base drag reduction can be achieved by afterbody boattailing[(2)], base bleed or base burning[(3,4)], some vortex suppression devices[(5)], and their combinations[(6)]. Such active or passive flow control techniques, basically, manipulate or alter the near-wake flowfield for an increase in base pressure and consequently reduce base drag. And these have been applied in somewhat empirical manners to date due to a lack of understanding of viscous-inviscid flow interactions between the near-wake flow and freestream.

Fig.1 shows the schematic diagram of the supersonic base flow and afterbody model under consideration in the present computation. The supersonic freestream expands through an expansion fan and at the base corner, and the wall boundary layer approaching to the base is separated at the corner and recompressed by compression waves at a certain downstream region. The interactions between two distinct flows inside and outside the separation lead to a free shear layer along the boundary of the flows and

† 안동대학교 기계공학부
E-mail: kimhd@andong.ac.kr
TEL: (054) 820-5622 FAX: (054) 823-5495
* 안동대학교 기계공학부
** School of Aeronautical Engineering, The Queen's University of Belfast, United Kingdom

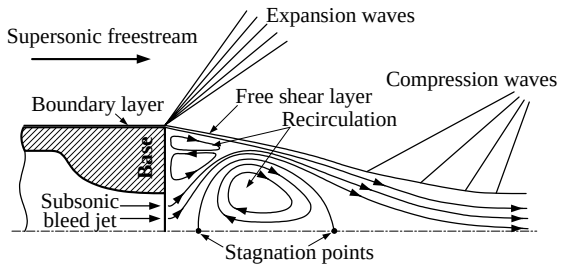

Fig.1 Supersonic base flow with mass bleed

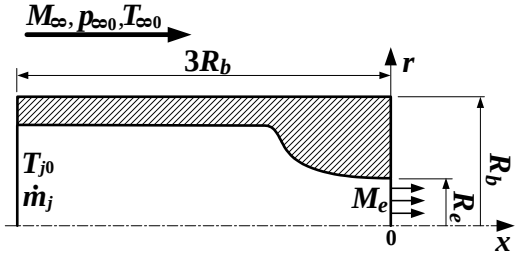

Fig.2 Afterbody model

recirculating flows inside the separation. In the presence of low mass bleed into the separated region, such flow features can be significantly changed depending on the bleed mass flow rate for a given freestream Mach number and afterbody geometry.(7)

According to a computational work(1) conducted by Sahu et al. using thin-layer Navier-Stokes equations, at transonic speeds of Mach 0.9 to 1.2, the use of mass bleed can reduce base drag by 40-80 %. However, the drag does not continuously decrease with increased mass bleed. An experimental study performed by Bourdon and Dutton(8) reported that an optimum condition giving the maximum base pressure was observed at a certain bleed mass flow rate for the given freestream Mach number of about 2.5. This important feature must be validated with computational results to be applied with reliability.

In the present study, a compressible base flow in a supersonic freestream at Mach 2.47 was numerically investigated. Computations have been conducted using axisymmetric mass-averaged Navier-Stokes equations with the standard k-ω turbulence model. The results are validated with experimental data(9) and also supported by detailed flow visualization to give a better understanding of the physics of base flows controlled by a bleed jet.

2. Numerical Simulations

2.1 Afterbody Model

Fig. 1 shows the afterbody model used in the present CFD (computational fluid dynamics) analysis, taken from Ref.(9) for validation. In the figure, M, p, T are Mach number, pressure and temperature, and subscripts 0, j and ∞ represent a total state, bleed jet and freestream respectively. The bleed mass flow rate $\dot{m}_j$ and the Mach number at the orifice exit M_e are given for the mass bleed under consideration. Regarding the model dimensions, the diameters of the model and orifice exit are given as R_b and R_e respectively. The afterbody is taken for computations only up to a length of $3R_b$ from the origin that is the center of the orifice exit. The details of model geometry and properties given to specify flow conditions are shown in Table 1, where $\mathrm{Re}_{\mathrm{unit}}$ is the unit Reynolds number of the freestream.

Table 1 Details of CFD model

M_∞	2.47	$\mathrm{Re}_{\mathrm{unit}}$	46×10^6 m^{-1}
$p_{\infty 0}$	470 kPa	T_{j0}	293 K
p_∞	28.8 kPa	R_b	31.75 mm
$T_{\infty 0}$	300 K	R_e	12.70 mm

2.2 Numerical methods

The present CFD study adopted a commercial computational code, FLUENT 5, in order to analyze complex flow interactions between a supersonic base flow and a subsonic bleed jet. Axisymmetric compressible mass-averaged Navier-Stokes equations governing the flowfield around an afterbody with mass bleed at the base were solved. The governing equations are discretized spatially and temporarily using a fully implicit finite volume scheme and a multi-stage Runge-Kutta scheme(10) respectively in the code. To obtain accurate solutions for the base flow including separation regions, wakes, strong free shear layers and wave systems, suitable turbulence modeling is indispensable. Therefore, preliminary computations were carried out for several turbulence models and wall functions.

2.3 Computational Domain and Analysis

Fig. 3 shows the grid layout near the afterbody model and brief information of the computational

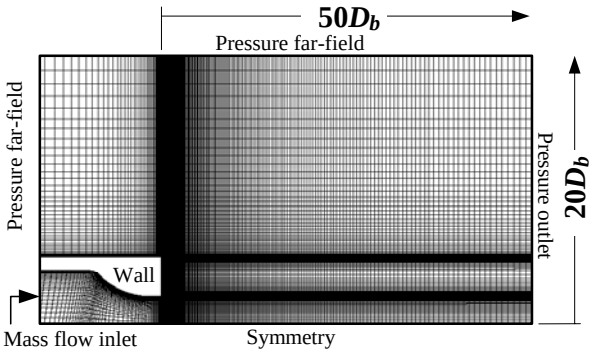

Fig.3 Computational grids

domain used in the current CFD analysis with boundary conditions applied. It has been found that about 50,000 nodes are required to get grid-independent solutions with the computational domain used. Grids were clustered in the regions with large gradient near model surfaces and downstream of the base where the separation of a turbulent boundary layer and wave systems are expected to exist.

The computational domain were set up with dimensions of $50D_b$, where D_b is the model diameter, downwards from the base and $20D_b$ upwards from the model axis to ensure freestream conditions and thus to obtain better convergence. Freestream boundaries are identified with a combination of the pressure far-field and pressure outlet conditions as shown in the figure. Preliminary test showed better convergence could be achieved using it rather than the use of the pressure far-field condition at all outer boundaries. To specify the freestream condition, the Mach number and static properties were applied to the boundaries.

Bleed air is injected through an orifice into the near wake region behind the model base. For obtaining various characteristics of mass bleed, the bleed mass flow rate $\dot{m}_j$ applied to the mass flow inlet boundary is changed corresponding to the injection parameter I given as follows.

$$I = \frac{\dot{m}_j}{A_b \rho_\infty U_\infty} \tag{1}$$

where A_b is the base area, and ρ_∞ and U_∞ are the density and velocity of the freestream. With $\dot{m}_j$, total temperature and static pressure are given at the inlet boundary. Adiabatic and no-slip conditions are applied to the wall boundaries, and a symmetry boundary condition is applied to the domain axis. The properties used for the boundary conditions mentioned are given in Fig.1 and Table 1.

Regarding testing conditions, I was changed from 0.005 to 0.032 for the fixed model geometry and freestream conditions. With a proper grid size and computational domain obtained through preliminary tests, basically, solutions were considered converged when the residuals of mass and momentum equations dropped below 10^{-4}. The mass imbalance was also checked for flow inlet and outlet boundaries and it was kept to be less than ±0.1%.

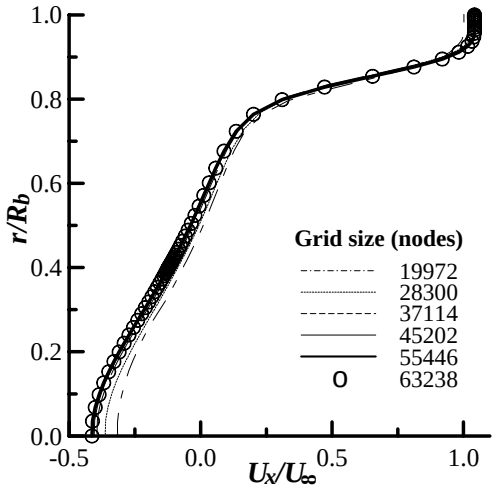

Fig. 4 Velocity profiles at x/R_b = 1.0 with a change in grid size (I = 0.0038)

Table 2 Base pressure (I = 0.00038)

Turbulence Model		p_b/p_∞
Standard k-ω		0.602
RNG k-ε	SWF	0.569
	NWF	0.572
RSM	SWF	0.571
	NWF	0.580
Experimental, Ref.(9)		0.592

3. Results and Discussion

For I = 0.0038, Fig.4 shows grid dependency on the solution given here as axial velocity profiles at x/R_b =

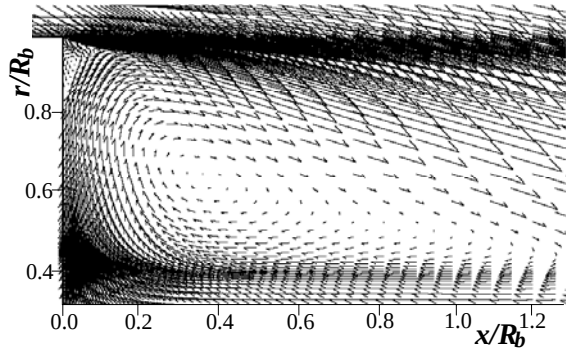

(a) I = 0

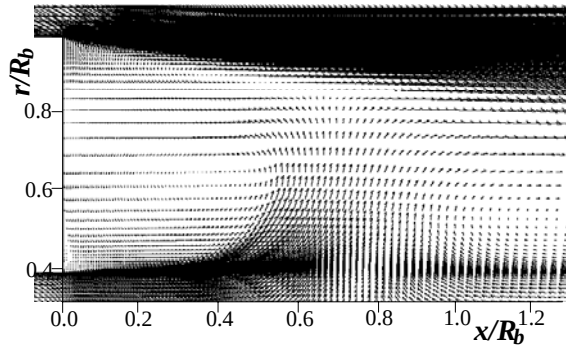

(b) I = 0.0113

Fig.5 Velocity vectors near the base

1.0 for several grid sizes. The velocity profiles presented have been computed using the standard k-ω turbulence model. The radial distance r and the axial velocity U_x were normalized by R_b and U_∞ respectively. The grid size has been tested in a range of about 20,000 to 63,500 nodes. In the figure, the profile inside the back flow region near the axis (r/R_b = 0.0) has a relatively significant change for the grid sizes tested. Because grid sizes with more than 45,202 nodes give no more change in the profile, it is considered that 45,202 nodes are enough to have grid independent solutions for the given value of I. For larger I values, in this approach, it has been found that about 50,000 nodes can be used to simulate the flowfields under consideration.

With a proper grid size obtained through the approach aforementioned, several turbulence models and wall functions have been tested at I = 0.0038, and base pressure values p_b normalized by p_∞ are given in Table 2. In comparison of computed values and a measured value taken from Ref.(9), the standard k-ω turbulence model resulted in the closest prediction of base pressure. The results also indicate that the effect of wall functions on base pressure predictions is insignificant for the geometry and testing conditions

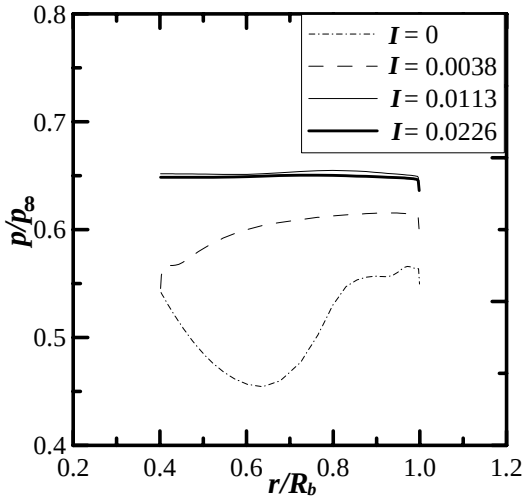

Fig.6 Base pressure distributions with base bleed

used in the present computations.

Fig.5 present mean velocity vectors near the base with and without base bleed. In the figures, axial and normal distances are normalized by R_b. Without base bleed (The whole base region was treated as a wall.), a large and strong recirculating flow is observed. In general, for aerodynamic bodies, base drag rises due to a decrease in base pressure depending on such separation. As mass is injected into the separated region (I = 0.0113), the recirculation near the model base becomes significantly weakened.

With a change in the injection parameter I, Fig.6 shows base pressure distributions. The pressure values estimated along the base (r/R_b = 0.4 to 1.0) are non-dimensionalized by the freestream pressure p_∞. The base pressure level, generally, increases with increased mass bleed. Without base bleed, a large pressure gradient is existent in the region between r/R_b = 0.4 and 0.85 due to a strong circulating flow along the base as observed in Fig.5(b). As I increases, however, such a gradient becomes smaller, consequently being similar for I = 0.0038 and 0.0113. It implies that the flow pattern downstream of the base will not be considerably different from a certain value of I.

Comparisons between computationally and experimentally visualized bases are given in Fig.7 and Fig.8. In Fig.7, computed Schlieren images (upper side) are given with corresponding axial velocity contours valued by U_x/U_∞. The experimental visualization presented in Fig.8 is taken from Ref.(8). The images were obtained using an acetone planar laser-induced fluorescence (PLIF) technique. In order of blue, white and red, average fluorescence intensity

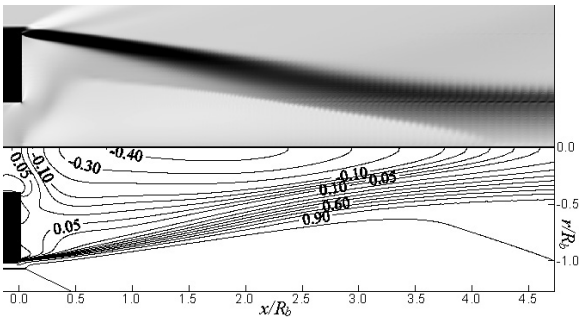

(a) I = 0.0038

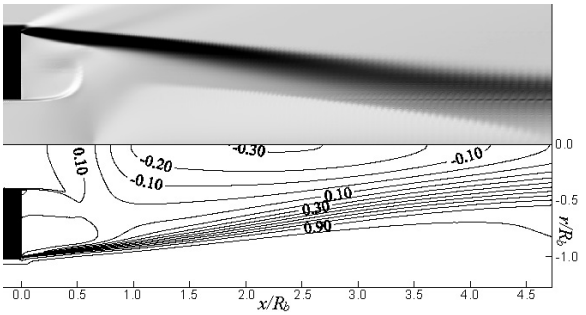

(b) I = 0.0113

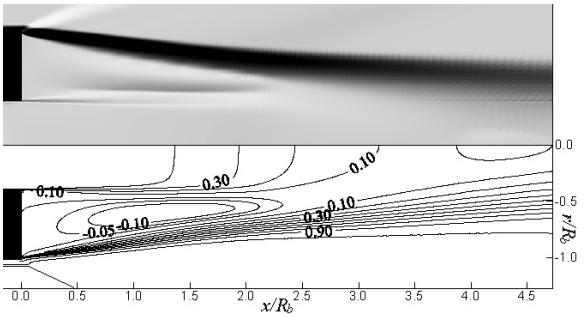

(c) I = 0.0226

Fig.7 Computed Schlieren images and U_x/U_∞ contours

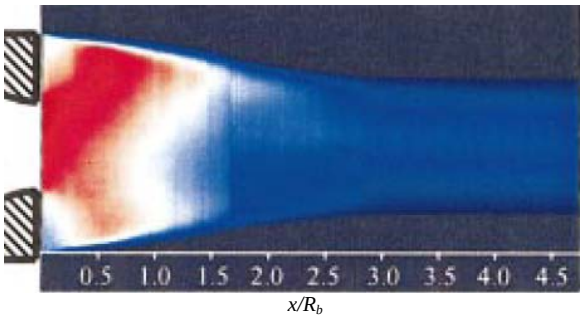

(a) I = 0.0038

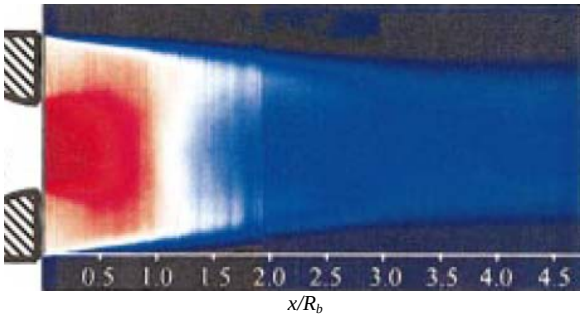

(b) I = 0.0113

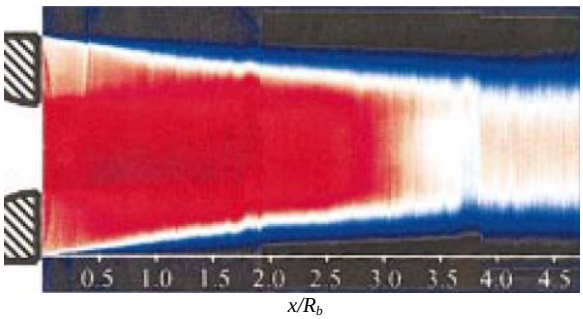

(c) I = 0.0226

Fig.8 Experimental visualization with average acetone laser-induced fluorescence signal, Ref.(8)

increases. The detailed description of the technique can be referred to the reference.

The supersonic freestream expands at the corner of the model and the wall boundary layer separates there, then forming an ensuing free shear layer. The separated flow is then reattached at a certain downstream location by a series of compression waves for the cases presented here. Inside the separated region, two major recirculation areas are observed near the base and axis. With increased mass bleed, the x-directional directivity of the bleed jet increases, and then the upper recirculation (near the base) becomes stronger and the lower recirculation (near the axis) becomes weaker. These flow characteristics can be apparently shown though axial velocity contours. The lower recirculation moves downstream as I increases. At I = 0.0226, the

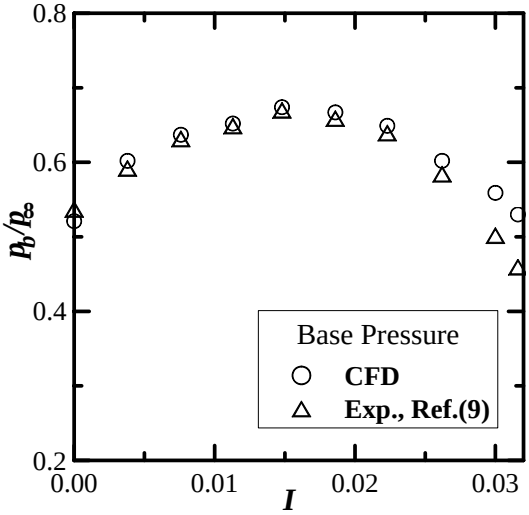

Fig.9 Area-averaged base pressure

lower separation is almost negligible. Therefore, it is expected that a further increase in I completely moves away the separation from the axis. Computed Schlieren images and PLIF images are in qualitative accordance but, for the cases with I = 0.0038 and 0.0113, the recirculation near the axis computed is placed further upstream than measured results.

In Fig.9, base pressure obtained through the present CFD method and an experiment[9] are presented with I. The base pressure values shown in the figure are obtained by the production of the area of the base wall and the pressure force acting on the wall. Except no-bleed case (I = 0), computed base pressure is slightly overestimated. And the difference becomes relatively significant when $I \geq 0.025$. For the overall tested injection parameter range, however, CFD and experimental results show reasonable agreement. It is interesting to note that an optimum condition with a maximum base pressure can be obtained as increasing mass bleed. For the given freestream conditions and geometry in the present CFD study, it occurs at I = 0.0148 as estimated in the experiment. From the results discussed in this paper, it is understood that an increase and a decrease in base pressure as changing mass bleed are decided by a relation between the recirculation regions deformed depending on I rather than I itself. Therefore, further investigations regarding various afterbody geometry and mass bleeding methods are required for providing systematic knowledge base on the base bleed problem.

4. Conclusions

The base flow with and without mass bleed in a Mach 2.47 freestream was investigated by CFD as a tool. Axisymmetric, compressible mass-averaged Navier-Stokes equations were computed using a two-equation turbulence model, standard k-ω, a fully implicit finite volume scheme and multi-stage Runge kutta scheme. The injection parameter was changed to offer various characteristics of subsonic bleed jet flows injected into the separated region behind the model base.

The validation results given as the computed Schlieren images and base pressure values are in good accordance with PLIF images and measured base pressure taken from a past experiment. As the injection parameter increases, the strength and the location of the recirculation formed near the base and the model axis were significantly changed. The quantitative valuse were observed through axial velocity contours. Through base pressure evalutations, the optimum condition providing minimum base drag could be correctly predicted.

References

(1) Sahu, J. and Nietubicz, C. J., 1985, “Navier-Stokes Computations of Projectile Base Flow with and without Mass Injection,” AIAA J., Vol.23, No.9, pp.1348-1355.

(2) Viswanath, P. R. and Patil, S. R., 1990, “Effectiveness of Passive Devices for Axisymmetric Base Drag Reduction at Mach 2,” J. Spacecraft and Rockets, Vol.27, No.3, pp.234-237

(3) Wood, C. J., 1967, “Visualisation of an Incompressible Wake with Base Bleed,” J. Fluid Mechanics, Vol.29, No.2, pp.259-272.

(4) Murthy, S. N. B., and Osborn, J. R., 1976, “Base Combustion Effects on Base Pressure,” Aerodynamics of Base Combustion, Progress in Astronautics and Aeronautics, AIAA, Vol.40, pp.307-338.

(5) Nash, J. F., Quincey, V. G. and Callinan, J., 1966, “Experiments on Two-Dimensional Base Flow at Subsonic and Transonic Speeds,” ARC R&M 3427.

(6) Addy, A. L., 1970, “Thrust-Minus-Drag Optimization by Base Bleed and /or Boattailing,” J. Spacecraft and Rockets, Vol.7, No.11, pp.1360-1362.

(7) Bowman, J. E. and Clayden, W. A., 1967, “Cylindrical Afterbodies in Supersonic Flow with Gas Ejection,” AIAA J., Vol.5, No.8, pp.1524-1525.

(8) Bourdon, C. J. and Dutton, J. C., 2003, “Visualization of a Central Bleed Jet in an Axisymmetric, Compressible Base Flow,” Physics of Fluids, Vol.15, No.2, pp.499-510.

(9) Mathur, T. and Dutton, J. C., 1996, “Velocity and Turbulence Measurements in a Supersonic Base Flow with Mass Bleed,” Vol.34, No.6, pp.1153-1159.

(10) Jameson, A. Schmidt, W. and Turkel, E., 1981, “Numerical Solution of the Euler Equations by Finite Volume Methods Using Runge-Kutta Time-Stepping Schemes,” AIAA Paper 81-1259.